Acta Oceanol. Sin., 2018, Vol. 37, No. 2, P. 66–75
DOI: 10.1007/s13131-017-1125-9
http://www.hyxb.org.cn
E-mail: hyxbe@263.net

Tectono-thermal evolution of the Liwan Sag, deepwater area in the Zhujiang River Mouth Basin, northern South China Sea

TANG Xiaoyin[1]*, HUANG Shaopeng[1], YANG Shuchun[3], JIANG Guangzheng[2], JI Mo[3], HU Shengbiao[2]

[1] Geothermal and Environmental Research Laboratory, Xi'an Jiaotong University, Xi'an 710049, China

[2] State Key Laboratory of Lithospheric Evolution, Institute of Geology and Geophysics, Chinese Academy of Sciences, Beijing 100049, China

[3] CNOOC Research Institute, Beijing 100027, China

Received 27 February 2017; accepted 10 May 2017

Abstract

The Liwan Sag, with an area of 4 000 km^2, is one of the deepwater sags in the Zhujiang River (Pearl River) Mouth Basin, northern South China Sea. Inspired by the exploration success in oil and gas resources in the deepwater sags worldwide, we conducted the thermal modeling to investigate the tectono-thermal history of the Liwan Sag, which has been widely thought to be important to understand tectonic activities as well as hydrocarbon potential of a basin. Using the multi-stage finite stretching model, the tectonic subsidence history and the thermal history have been obtained for 12 artificial wells, which were constructed on basis of one seismic profile newly acquired in the study area. Two stages of rifting during the time periods of 49–33.9 Ma and 33.9–23 Ma can be recognized from the tectonic subsidence pattern, and there are two phases of heating processes corresponding to the rifting. The reconstructed average basal paleo-heat flow values at the end of the rifting events are ~70.5 and ~94.2 mW/m^2 respectively. Following the heating periods, the study area has undergone a persistent thermal attenuation phase since 23 Ma and the basal heat flow cooled down to ~71.8–82.5 mW/m^2 at present.

Key words: tectono-thermal evolution, thermal history, heat flow, deepwater area, Liwan Sag

Citation: Tang Xiaoyin, Huang Shaopeng, Yang Shuchun, Jiang Guangzheng, Ji Mo, Hu Shengbiao. 2018. Tectono-thermal evolution of the Liwan Sag, deepwater area in the Zhujiang River Mouth Basin, northern South China Sea. Acta Oceanologica Sinica, 37(2): 66–75, doi: 10.1007/s13131-017-1125-9

1 Introduction

Petroleum exploration activities in deepwater and ultra-deepwater environments are becoming increasingly important since the 1990s. More than 20 large oil-bearing deepwater basins have been found in the slope and abyssal plain of the Gulf of Mexico, the South America margin, the West Africa margin, and the East Asian seas (Pettingill and Weimer, 2002; Khain and Polyakova, 2004). The South China Sea (SCS) is one of the largest marginal seas in the rim of the western Pacific Ocean. Its evolution and hydrocarbon potential have attracted great attention of geoscientists all over the world. Inspired by the worldwide success of deep water hydrocarbon exploration in recent decades, the exploration and related scientific research have been advanced to the deepwater areas of the northern SCS, starting from the Baiyun Sag (BYS) in the southern Zhujiang River (Pearl River) Mouth Basin (ZRMB). A significant discovery of the LW 3-1 gas field was made in April 2006, which started the deepwater oil and gas exploration in China. In the wake of LW3-1gas field, the exploration success in oil-gas fields of LH34-2 and LH29-1 has assured the huge hydrocarbon resource potential in the deepwater areas of the ZRMB (Zhu et al., 2012).

The study area, Liwan Sag (LWS), lies in the southeast of the Baiyun Sag and closely to the continent-ocean boundary of the SCS, with a total area of 4 000 km^2, water depth over 2 000 m (Xie et al., 2013). This area is located tectonically in the conjunction of Eurasian, Indo-Australian, Pacific and Philippine Plates (Fig. 1a). As a newly discovered sag, the Liwan Sag is not well studied, and no well has been drilled in this area so far. Only several studies on the LWS have been reported, which mainly focused on the tectonic evolution (Ji et al., 2014), and the source rock characteristics (Miao et al., 2013). A thorough understanding of the petroleum geology of deepwater basins is critical during the initial exploration stage because of the high commercial threshold and geological risks. Thermal history is one of the fundamental facets of petroleum systems as it controls the timing of hydrocarbon generation and expulsion (Carminati et al., 2010; Hudson and Hanson, 2010). Up to date, no work concerning the thermal history evolution of the Liwan Sag has been carried out. However, such information is critical to understand not only the tectonic evolution but also the hydrocarbon potential of the study area.

With the proceeding of hydrocarbon exploration to deepwater areas in recent years, a large quantity of new 2D multi-channel seismic data have been acquired. In order to understand the tectono-thermal evolution and geodynamics of the Liwan Sag, we attempt to analyze its Cenozoic tectonics and reconstruct its thermal history in this study, based on the newly interpreted, yet unpublished 2D multi-channel seismic profiles.

Foundation item: The Program of the Key Technologies for Petroleum Exploration in Deep Oceanic Areas under contract No. 2011ZX05025-006-05; the Chinese Postdoc Fund, No. 58 General Fund, 2015 under contract No. 2015M582636; the National Natural Science Foundation of China under contract No. 41602251.

*Corresponding author, E-mail: xytang2015@xjtu.edu.cn, xytang2015@sina.com

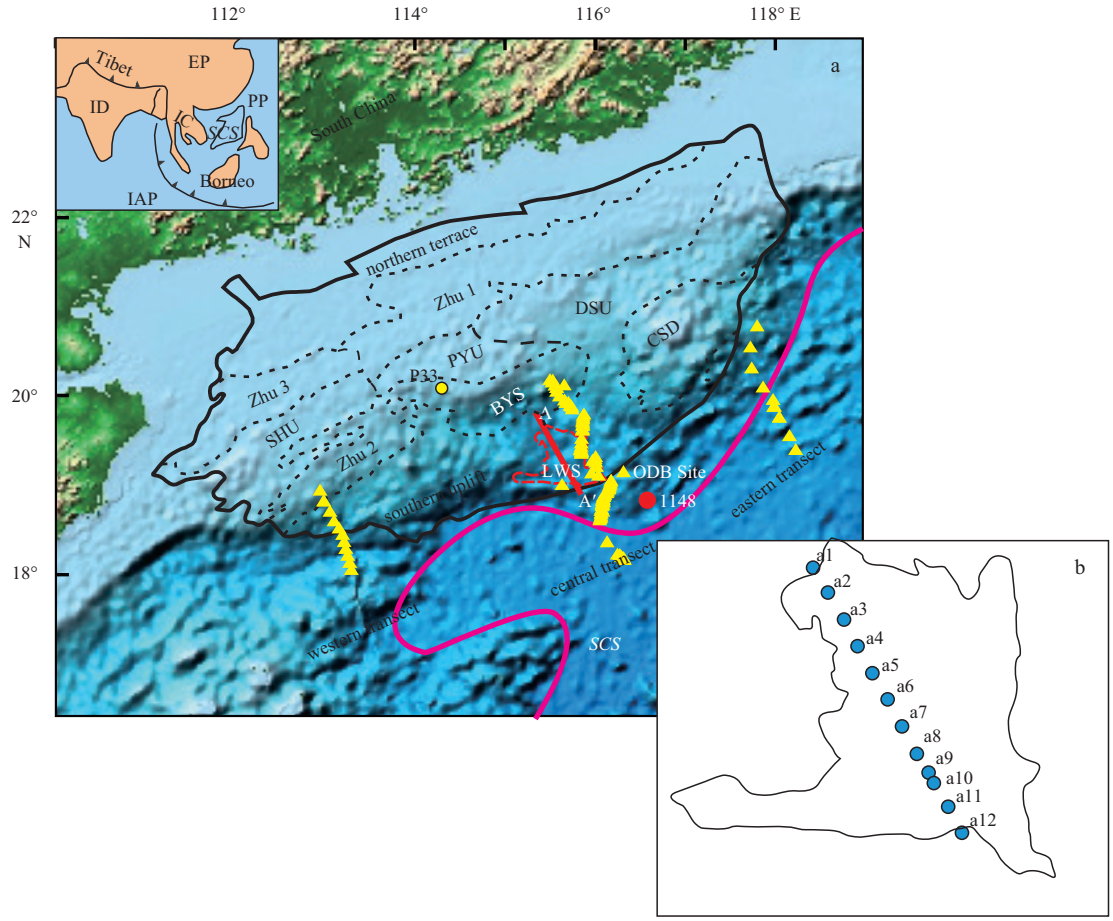

Fig. 1. Geographical location and tectonic settings of the Liwan Sag (a) and locations of artificial wells along the seismic profile (b). In Fig. 1a, EP represents Eurasian Plate, PP Pacific Plate, IAP India Australian Plate, IC Indochina Block, ID India Block, SCS South China Sea, SHU Shenhu Uplift, PYU Panyu Uplift, DSU Dongsha Uplift, BYS Baiyun Sag, CSD Chaoshan Depression, and LWS Liwan Sag. Red line denotes the seismic profile used in this study. Pink line represents the continent-ocean boundary. Yellow triangles represent the three probe heat flow sections obtained in Sino-USA joint projects (Nissen et al., 1995b). Red and yellow circle show the positions of ODP Site 1148 and drilling Well P33, respectively. In Fig. 1b, blue circles denote the artificial wells.

2 Geological setting

The ZRMB is the largest sedimentary basin on northern of the SCS, with a total area of 200 000 km^2. The basin consists of two depression zones sandwiched by three uplift zones, namely from north to south, the northern terrace, the northern depression zone consisting of Zhu 3 and Zhu 1 Depressions, the central uplift zone consisting of Shenhu, Panyu, and Dongsha Uplifts, the southern depression zone consisting of the Zhu 2 and Chaoshan Depressions (Fig. 1). The Liwan Sag discovered recently is situated in the Zhu 2 Depression and very close to the continent-ocean boundary of the South China Sea. The crust that underlain the ZRMB thins from ~30 km near the coast in the north to ~11 km near the deep-sea basin in the south (Nissen et al., 1995a; Kido et al., 2001; Huang et al., 2005). Beneath the centers of sedimentary depressions, the Moho surface shoals significantly, for example, the crust thins rapidly to less than 7 km under the center of the Baiyun Sag and less than 9 km under the center of the Liwan Sag (Hu et al., 2009).

A general Cenozoic stratigraphic column of the deepwater area of the ZRMB is presented in Fig. 2. The Wenchang Formation consists mainly of gray-black, organic-rich lacustrine shale with sandstone inter-beds. The Enping Formation is dominated by fluvial-lacustrine-paludal shale, sandstone, and thin coal beds. The major source rocks in the ZRMB were developed during the deposition of the Wenchang and Enping Formations (Chen and Pei, 1993; Dai and Pang, 1999; Zhu et al., 1999). Sediments in the Oligocene Zhuhai Formation are transitional (alternatively coastal and littoral) and contain both source rocks and reservoirs. The Zhujiang Formation contains carbonate sediments of the Dongsha Uplift and marine shale in depression areas. The Hanjiang Formation is composed mainly of pro-delta and shelf shale that act as regional seal rocks. The Yuehai and Wanshan Formations and Quaternary sediments are open-marine shelf deposits.

Several episodes of Cenozoic tectonic events have been recognized in the deepwater area of the ZRMB (Fig. 2). These are the first Zhuqiong Event and second episode Zhuqiong Event at 49 Ma and 38 Ma, respectively, the Nanhai Event at early Oligocene, the Baiyun Movement (possibly related to ridge jump) at the Paleogene/Neogene boundary, and the Dongsha Event (uplifting possibly related to the docking of Philippine archipelago) in Late Miocene (Dong et al., 2009; Zhou et al., 2009). Under the influence of the multi-episode tectonic movement, the stretching/rifting process of the study area is episodic (Ru and Pigott, 1986; Zhou et al., 1995; Dong et al., 2009).

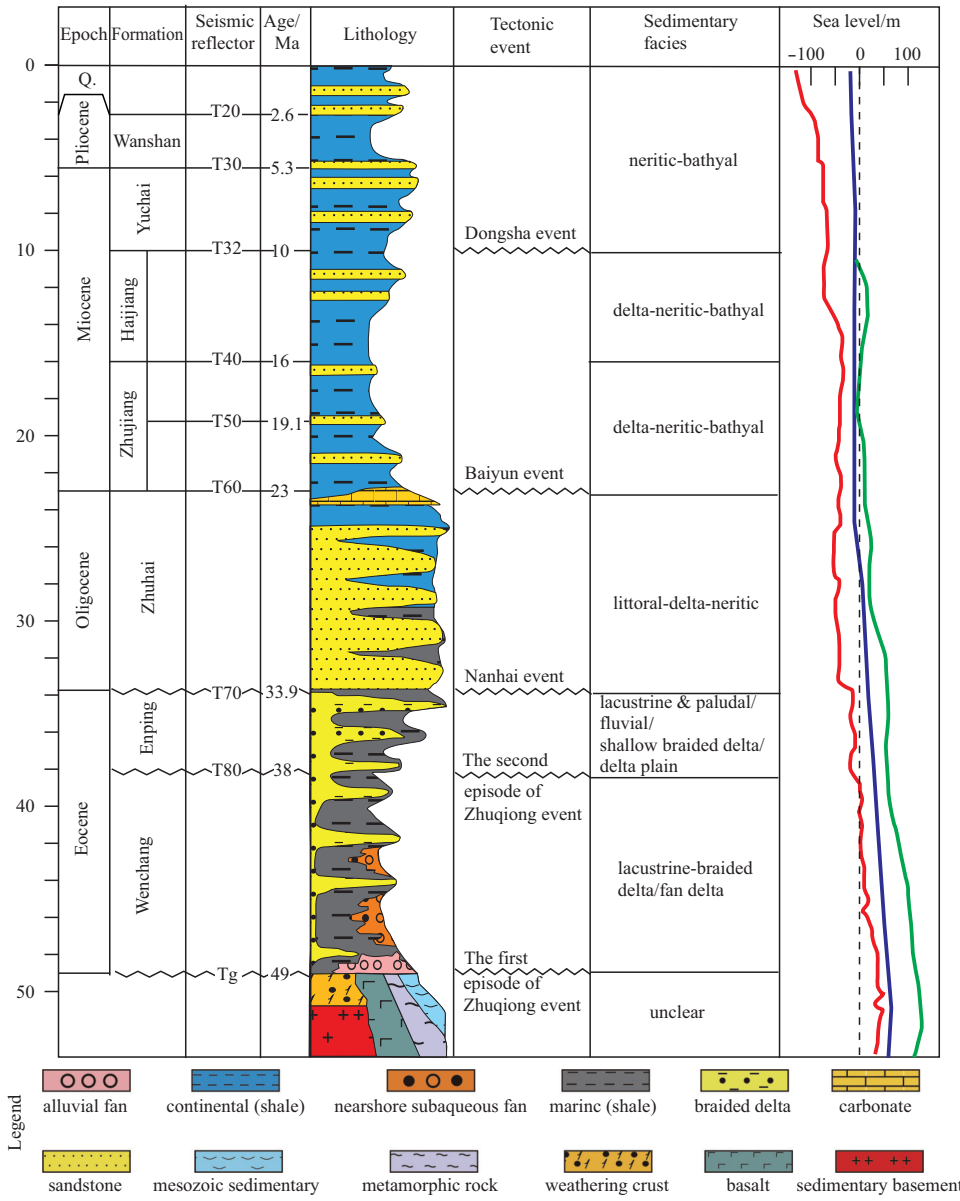

Fig. 2. Stratigraphic column, seismic reflectors, major tectonic events, sediment facies, and sea level change curves of the deepwater area of the Zhujia River Mouth Basin summarized from different sources (Dong et al., 2009; Ding et al., 2013; Chen, 2014; Xie et al., 2014). The red, blue, and green curves, of sea level change are from Cramer et al. (2009), Miller et al. (2011), and Kominz et al. (2008), respectively.

3 Data and methods

3.1 *Data and sources*

3.1.1 *Seismic profiles*

In recent years, great effort has been devoted to investigate deep structure of the LWS. In sequence stratigraphic analysis for the LWS conducted by the CNOOC during 2009–2010, the main boundaries were identified in the Cenozoic sediments, and the depth of these boundaries were obtained by time-depth conversion using cubic polynomial functions. These data are the bases for this study. In order to understand the tectono-thermal history, a set of artificial wells were constructed based on the seismic line AA′, see Fig. 1 for its location. Figure 3 shows the structure and strata information of the seismic line. Seismo-stratigraphic interpretation carried out by the CNOOC produced the following main stratigraphic horizons and ages: Tg–T8 (49–38 Ma), T8–T7 (38–33.9 Ma), T7–T6 (33.9–23 Ma), T6–T5 (23–19.1 Ma), T5–T4 (19.1–16 Ma), T4–T32 (16–10 Ma), T32–T3 (10–5.3 Ma), T3–T2 (5.3–2.6 Ma), and T2–seabed (2.6–0 Ma). Tg is the top of the basement; T7 approximates the Nanhai movement at 33.9 Ma; and T6 represents the Paleogene/Neogene boundary at 23 Ma. The main tectonic events and their associated seismic reflectors are shown in Fig. 2.

3.1.2 *Wells*

Up to date, there is no well data available in the Liwan Sag. Drilling Well P33 (Zhou et al., 2009; Chen, 2014), which located in the neighboring BYS (location see Fig. 1), has been used for lithology information and subsidence calibration.

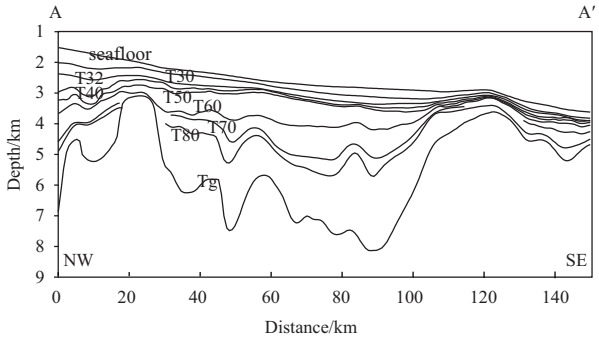

Fig. 3. Interpreted seismic section AA′ across the Liwan Sag showing the strata information. The ages for stratigraphic horizons are according to the International Chronostratigraphic Chart v2013/01 (Cohen et al., 2013), with Tg corresponding to 49 Ma, T8 to 38 Ma, T7 to 33.9 Ma, T6 to 23 Ma, T5 to 19.1 Ma, T4 to 16 Ma, T32 to 10 Ma, T3 to 5.3 Ma, and T2 to 2.6 Ma.

3.1.3 *Present-day heat flow*

Present-day heat flow, which can provide necessary constraints on the thermal history reconstruction, is the final episode of the entire scenario of basin tectono-thermal evolution, and the only one which may be measured directly (He et al., 2001, 2002). As of yet, no heat flow has been published in the LWS. Fortunately, heat flow data in the adjacent areas may provide us with some valuable information.

In the slope area of the SCS, three probe heat flow sections were obtained in two Sino-USA joint projects (see Fig. 1 for the location). Heat flow values on the eastern slope range from 67 to 91 mW/m^2, with an average of 78.8 mW/m^2. The heat flow range of the middle section is 59.2–162.6 mW/m^2, with an average of 83.6 mW/m^2. Heat flow values on the west section vary between 8 mW/m^2 and 121 mW/m^2, with an average of 73.3 mW/m^2 (Nissen et al., 1995b). According to the middle section, heat flow values on the east of the LWS range from 69.3 to 96 mW/m^2, with an average of 77 mW/m^2. The geothermal gradient of ODP LEG184-1148, which lies on the southeast of the LWS (see Fig. 1 for the location), is about 83°C/km (Wang et al., 2000). Based on the reported thermal conductivity, the average thermal conductivity is ~1.03 W/(m·°C), so the heat flow value is about 85.5 mW/m^2.

3.2 *Methods and parameters*

3.2.1 *Tectonic subsidence estimation*

Tectonic subsidence is defined as the vertical motion (positive downward) of basement at a site that is induced by tectonic forces such as thermal contraction, tectonic deformation, and dynamic topography. In order to obtain tectonic subsidence information, corrections need to be made for the effects of compaction and sediment loading, changes in paleo-water depth, and global sea level changes. To recover the tectonic component of subsidence in the Liwan Sag, 12 artificial wells were constructed along the profile AA′, and the back-stripping technique (Steckler and Watts, 1978) was used.

Water loaded tectonic subsidence was determined from the stratigraphic records adopting Airy isostasy to correct for the effect of sediment loading. Corrections for compaction were made by using porosity-depth relationships based on the observed lithology (Sclater and Christie, 1980). The lithology of each layer is determined by using the data from Well P33 as reference (Chen, 2014), which is located on the northern edge of the Baiyun Sag (see Fig. 1 for its location).

Because the study region is situated at the continental slope, where the maximum present-day bathymetry exceeds 2 000 m, the paleo-bathymetry potentially has an important effect in backs-tripping and deserves particular attention. The estimation of paleo-water depth is difficult, yet it is essential in order to accurately study subsidence history. A number of sources, such as benthic microfossils, faunal and floral assemblages, sedimentary facies and distinctive geochemical signatures, can give us information on paleo-bathymetry, but reliable estimates usually come from biostratigraphic data from wells (Bessis, 1986; Allen and Allen, 2005). Unfortunately, no drilling well with paleontological data is available in the Liwan Sag up to date. The ODP Site 1148, with present water depth of 3 294 m, is located nearly to the study area (see Fig. 1 for its location). Wang et al. (2000) reported that the early Oligocene sediments recovered from ODP Site 1148 are of deepwater facies, and this deepwater sequence likely continues downward in the seismic profile, indicative of the occurrence of a deepwater environment in the northern slope at least since the early Oligocene, probably even earlier (Wang et al., 2003; Wang, 2012). The detailed study of benthic faunas from ODP Site 1148 shows an obvious change of water depth from the upper bathyal shallower than 1 000 m in the earliest Oligocene (ca. 33.5–32 Ma) to 1 000–1 500 m in the late early Oligocene (ca. 32–27 Ma), lower bathyal between 1 500 m and 2 500 m in the late Oligocene to earlier middle Miocene (ca. 26–14 Ma), and depths similar to the present day (2 500–3 500 m) in the late middle Miocene (14 Ma) to the present (Zhao, 2005). Pang et al. (2007) reported a similar changing trend in the sediment sequence from the Baiyun Sag, which was closely next to the Liwan Sag, indicating a transition from shallow to deepwater conditions during this time span. Because there is no well penetrating the sediment basement at the northern continental slope of the SCS available, paleo-bathymetry older than the Oligocene can only be deduced from sedimentary facies of shallow-water wells (Xie et al., 2006). Keeping the above knowledge in mind, here we estimate paleo-bathymetry by observing the following rules: (1) the seafloor depth defined by the seismic profiles accurately gives the present-day bathymetry for any given site; (2) the water depth at the very beginning of rifting (i.e., 49 Ma) is assumed to be zero; (3) the estimates for the artificial wells are constrained by the results at ODP Site 1148 (Zhao, 2005). Though the eustatic sea-level fluctuation has less influence on back-stripping compared to the variations of paleo-bathymetry, a recent compilation of global long-term sea level change (Kominz et al., 2008; Cramer et al., 2009; Miller et al., 2011) has been incorporated in back-stripping in order to make the subsidence study integrity.

3.2.2 *Stretching factor and heat flow estimation*

Although much research has been conducted to estimate stretching factors on the northern margin of the SCS, the results were based on either the one-stage finite stretching model (Su et al., 1989; Shi et al., 2005) or the instantaneous stretching model (Ru and Pigott, 1986; Clift and Lin, 2001). According to the study of Jarvis and McKenzie (1980), the assumption of instantaneous extension is valid only if the stretching duration is less than 20 Ma. Thus, the measuring stretching factor in terms of one-stage finite stretching mode or instantaneous stretching mode lead to considerable error, given that the ZRMB has experienced several stage of rifting and the entire extension duration lasted for over 30 Ma (Ru and Pigott, 1986; Zhou et al., 1995).

Herein, we choose the multi-stage finite stretching method (Chen et al., 2013; Tang et al., 2014) to understand the long-term

and multi-episodic extensional tectonics as well as the thermal history of the study area. This alternative approach is based on the finite stretching model proposed by Jarvis and McKenzie (1980) to avoid the problems caused by the assumption of instantaneous extension.

In this model, the theoretical tectonic subsidence is given by Jarvis and McKenzie (1980):

$$S(t)=A\left(1-\frac{1}{\beta}\right)-BQ(t), \tag{1}$$

where

$$A=\frac{t_c(\rho_m-\rho_c)}{\rho_m(1-\alpha T_m)-\rho_w}, \tag{2}$$

$$B=\frac{\alpha\rho_m}{\rho_w-\rho_m(1-\alpha T_m)}, \tag{3}$$

$$Q(t)=\int_0^a[T(z,t)-T(z,\infty)]\mathrm{d}z, \tag{4}$$

where $T(z,t)$ is the temperature of the lithosphere as a function of depth and time; $T(z,\infty)$ is the equilibrium temperature structure of the lithosphere; t_c and a are the crust and lithosphere thickness prior to stretching, respectively; ρ_w, ρ_c and ρ_m are seawater, crust and lithospheric mantle density, respectively; α is the thermal expansion coefficient; and T_m is the lithosphere basal temperature.

The relationship between strain rate $G(t)$ and stretching factor β is

$$\beta=\exp\left(\int_0^{\Delta t}G(t)\mathrm{d}t\right). \tag{5}$$

In this model, the temperature evolution consists of active rifting and its subsequent cooling stage. Temperature of the lithosphere at a rifting stage is governed by the heat conduction equation with an additional advection term (Jarvis and Mckenzie, 1980):

$$\frac{\partial T}{\partial t}+G(a-z)\frac{\partial T}{\partial Z}=\kappa\frac{\partial^2 T}{\partial Z^2}, \tag{6}$$

where T is temperature, t is time, κ is thermal diffusivity, and $G=\frac{\partial u}{\partial x}$ (u is the horizontal component of velocity field) is the vertical strain rate.

Assuming the lithosphere is in thermal steady state before rifting, the temperature is given by

$$T(z,\ t=0^-)=T_m(1-z/a). \tag{7}$$

The boundary condition for Eq. (7) is

$$T=\begin{cases}0, & z=a,\\ T_m, & z=0.\end{cases} \tag{8}$$

During the rifting stage, strain rate decays exponentially with time, and reach the value of zero at the end of rifting, that is

$$G(t)=\begin{cases}G_0\exp(-t/\Delta\tau), & 0\leqslant t\leqslant\Delta t_d,\\ 0, & t>\Delta t_d,\end{cases} \tag{9}$$

where G_0 is the strain rate at the beginning of rifting (t=0), $\Delta\tau$ decides the speed of the exponential decay, and Δt_d is the stretching duration.

In the post-rift stage, lithosphere stretching ceases and the thermal-perturbed lithosphere begins to cool. Thus, the above equation reduces to

$$\frac{\partial T}{\partial t}=\kappa\frac{\partial^2 T}{\partial z^2}. \tag{10}$$

The heat flow is then given by

$$q(t)=-k\frac{\partial T}{\partial u}|_{z=a}, \tag{11}$$

where k is the thermal conductivity.

To analyze the multi-episodic extension process, we generalize the original finite stretching model as follows. The lithospheric temperature structure at the end of a rifting cycle, which consists of active rifting and its subsequent cooling stage, is taken as the initial temperature structure of the following rifting event. In turn, the subsidence basement produced by the former rifting cycle is taken as the starting point of subsiding for the following rifting event. In terms of this structural and geothermal inheritance of the lithosphere, the following rifting event can naturally evolve from the preceding event without any artificial intervention (Chen et al., 2013).

The procedure for modeling based on the multi-episodic finite stretching model can be briefly summarized as follows: according to the back-stripping/observed subsidence curves and geological information, the divisions of the syn-rift and post-rift phases are determined for each rifting event. This stretching factor estimation involves calculating a number of theoretical subsidence curves using the multi-episodic finite stretching model, increasing the stretching factor by a small increment each time. The stretching factor which best fits the observed and calculated subsidence is regarded as the ideal factor for a corresponding rifting event. The cumulative/total stretching factor is obtained by the summation of individual stretching factors. Based on Eqs (5), (7), (8) and (9), we could obtain the temperature evolution during the rifting stage by solving Eq. (6). Taking the temperature at the end of rifting as the initial temperature for the subsequent cooling stage, the temperature evolution during the post-rift stage could be obtained by solving Eq. (10). Finally, the thermal history could be achieved by solving Eq. (11). The related parameters used in the present study are listed and defined in Table 1.

4 Results

4.1 *Tectonic subsidence and lithosphere-scale stretching factor*

The subsidence history at rifted continental margins recorded in stratigraphic data contains information that allows the amount of lithosphere stretching to be determined under the assumption of uniform extension. Using the traditional back-strip-

Table 1. Definitions and values of parameters used in this study

Symbol	Parameter	Value	Unit
a	lithospheric thickness	125	km
t_c	pre-rift thickness of continental crust	30	km
ρ_w	sea water density	1 030	kg/m^3
ρ_c	crust density at STP	2 800	kg/m^3
ρ_m	mantle density at STP	3 330	kg/m^3
T_m	temperature at base of lithosphere	1 350	°C
κ	thermal diffusivity of lithosphere	1.0×10^{-6}	m^2/s
α	lithosphere thermal expansion coefficient	3.28×10^{-5}	°C^{-1}
κ_c	crust thermal conductivity	3.1	W/(m·K)
κ_m	mantle thermal conductivity	2.9	W/(m·K)

Note: STP represents standard temperature and pressure. The crustal and mantle thermal conductivity are taken from He et al. (2001, 2002) and Chen (2014).

ping method (see Section 3.2.1), the tectonic subsidence curves for 12 artificial wells were obtained (Fig. 4). These curves represent the observed subsidence curves in Fig. 5. It is unrealistic to describe the subsidence history of all the wells with a uniform mode, due to the complexity of the extension process and inherent lateral heterogeneity of crust composition. However, a general subsidence pattern for most of the wells can be revealed as a two-stage rapid tectonic subsidence characterized by different subsidence rates, and succeeded by a slower subsidence stage. The first period of rapid subsidence occurred during 49 Ma to 33.9 Ma, with a deceleration at 38 Ma, while the second rapid period occurred during 33.9 Ma to 23 Ma.

The results of the subsidence analysis based on the multi-episodic finite stretching model are shown in Fig. 5. By matching the theoretical subsidence to the observed subsidence using a trial-and-error approach, the total stretching factors are determined to be 1.74–2.65 for all of the wells, with an average value of 2.26. The stretching factors for the first and second stage of rifting, as well as the total stretching factors, are listed in Table 2.

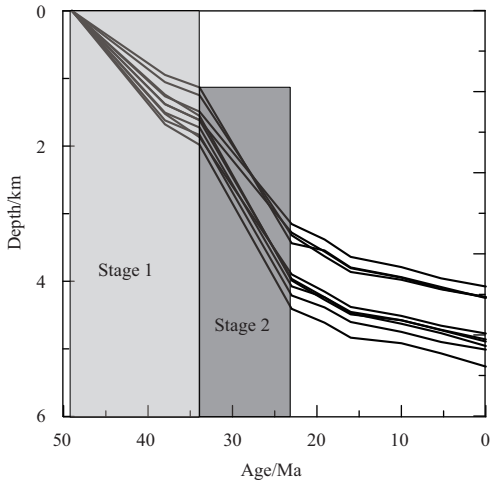

Fig. 4. An overview of the back-stripped tectonic subsidence curves for all the 12 artificial wells constructed based on profile AA′. Gray-shaded regions show the inferred rift stages.

4.2 *Thermal history*

Heat flow data (Fig. 6, Table 3) obtained in this study implies that the LWS underwent a two stages of heating, followed by a persistent cooling stage. At 49 Ma, the initial basal heat flow (heat flow through the base of the sedimentary basin) is ~54.9 mW/m^2, after the first stage of extension during the period of ~49–33.9 Ma, the basal heat flow had been raised to be ~65.3–78.4 mW/m^2 and further increased to the maximum of ~79.6–105.0 mW/m^2 at the end of the second stretching (~23 Ma); finally, the basin cooled down to the present-day heat flow of ~71.8–82.5 mW/m^2, with the average value of 78.5 mW/m^2.

The modeling results in this study show that the present basal heat flow of the LWS is about 71.8–82.5 mW/m^2. Revealed by the pseudo-wells distributed in the LWS, the Cenozoic sediment thickness is about 2.4–5.3 km. Given that the average radiogenic heat production of the Cenozoic sediment is 1.28 μW/m^3 (He et al., 2002; Yuan et al., 2009), the heat contribution from the Cenozoic sediment could be ~3.1–6.7 mW/m^2. Therefore, the surface heat flow of the LWS is about 74.9–89.3 mW/m^2, which is in accordance with the value reported by Nissen et al. (1995b) and the heat flow value of the ODP LEG184-1148.

5 Discussion

5.1 *Rifting stage division*

From Section 3.2.2, we know that the division of rifting stages strongly affects the estimation of the stretching factor and the subsequent heat flow. Previous geological and geophysical investigations suggest that there are several rifting events and associated thermal activities on the northern margin of the SCS, but how the rifting stages divided and when the post-rifting commenced is still controversial. Ru and Pigott (1986) suggested that the ZRMB has experienced at least three episodic rifting phases (late Cretaceous-Paleocene, late Eocene-early Oligocene, and middle Miocene) with two intervening stages of seafloor spreading, whereas Su et al. (1989) argued that the ZRMB was formed by a prolonged rifting event lasting from the late Cretaceous to late Oligocene with a minor event in the middle Miocene.

The classical stretching model of extensional basins includes a rapid or finite initial syn-rift subsidence followed by an exponentially decaying post-rift thermal subsidence (McKenzie, 1978; Jarvis and Mckenzie, 1980). The syn-rift and post-rift stages are separated by a breakup unconformity, which occurred at the time when seafloor spreading started (Falvey, 1974). According to the correlation of seafloor magnetic anomalies, the South China Sea opened at 32 Ma (Taylor and Hayes, 1983; Briais et al., 1993) or at 30 Ma on the revised geomagnetic timescale (Cande and Kent, 1995). This event, named as Nanhai Movement (T7) by Li (1993), was characterized by the breakup of the continental lithosphere and the start opening of the South China Sea. Given the classical model, the unconformity T7 should be regarded as the boundary of syn-rift and post-rift stages for the ZRMB (Peng et

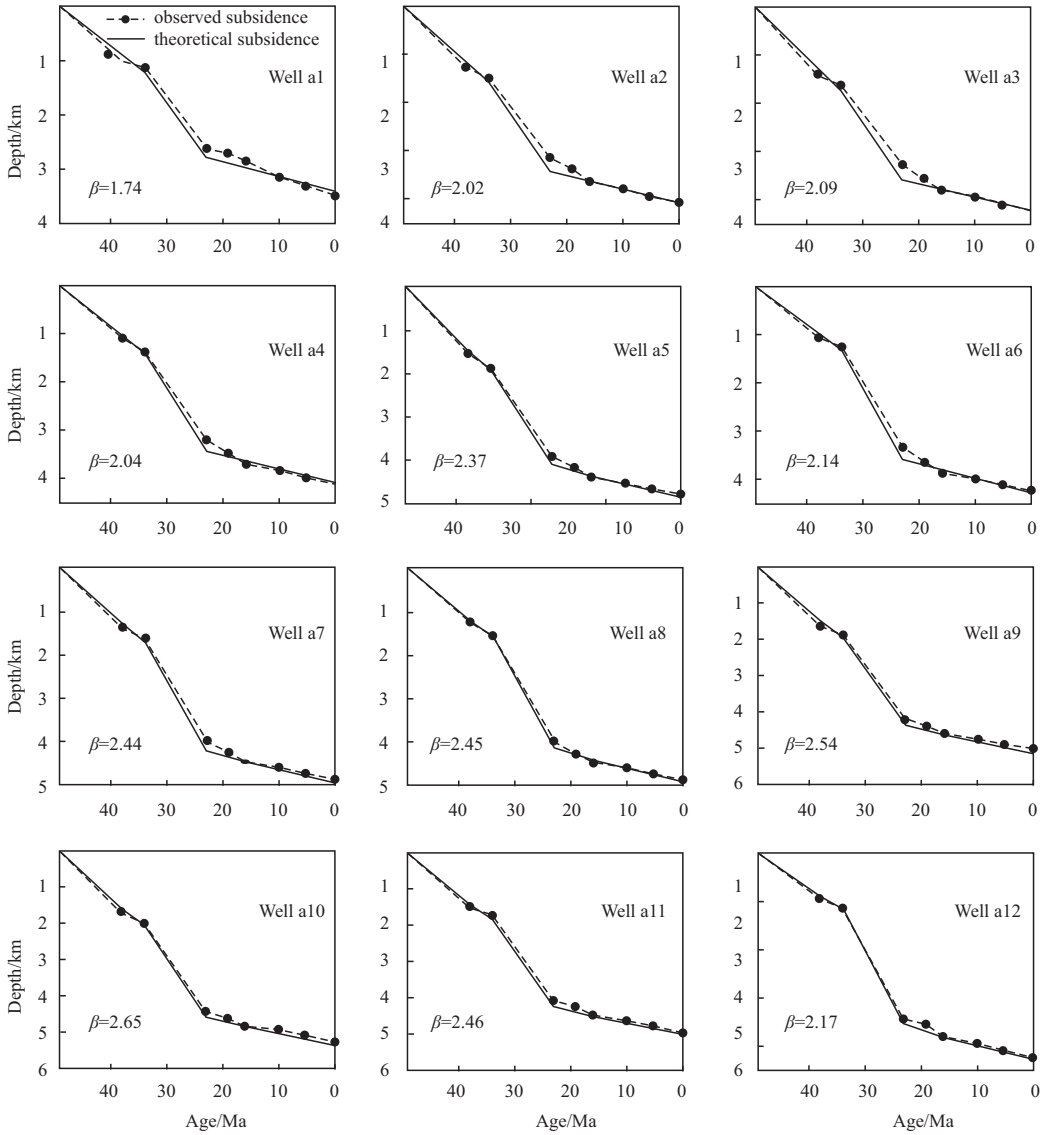

Fig. 5. Subsidence analysis for the 12 artificial wells in the Liwan Sag. The circles connected by the dashed lines indicate observed subsidence (from back-stripping), while the dark solid lines represent the theoretical subsidence predicted by the multi-episodic finite stretching model. The division of rifting stages for each well mainly depends on the time period during which a remarkable steepening of subsidence rate occurs. The best fitting stretching factors are tagged at the lower left corner of each panel.

Table 2. Stretching factor and subsidence rate during the two stages of rifting

Well	β_1	TSR1/m·Ma^{-1}	β_2	TSR2/m·Ma^{-1}	β
a1	1.30	0.07	1.34	0.12	1.74
a2	1.43	0.10	1.41	0.15	2.02
a3	1.49	0.11	1.40	0.15	2.09
a4	1.36	0.09	1.50	0.17	2.04
a5	1.60	0.12	1.48	0.19	2.37
a6	1.33	0.08	1.61	0.19	2.14
a7	1.49	0.11	1.64	0.22	2.44
a8	1.44	0.10	1.70	0.22	2.45
a9	1.61	0.12	1.58	0.22	2.54
a10	1.68	0.13	1.58	0.22	2.65
a11	1.55	0.11	1.59	0.22	2.46
a12	1.29	0.07	1.68	0.21	2.17
Average	1.46		1.54		2.26

Note: β_1 and β_2 represent the stretching factors for the rifting Stage 1 and rifting Stage 2, β the total stretching factor multiplied by the first and second one, and TSR1 and TSR2 the tectonic subsidence rate for rifting Stage 1 and rifting Stage 2, respectively.

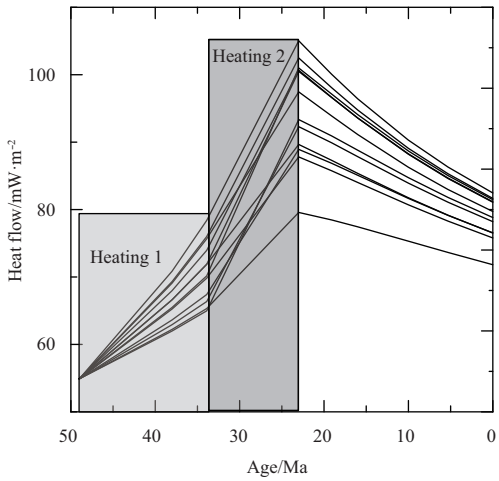

Fig. 6. Reconstructed thermal history for the artificial wells in the Liwan Sag.

al., 2005; Sun et al., 2005). However, based on an analysis of subsidence in ZRMB wells, Clift and Lin (2001) proposed that extension in the ZRMB continued for ~5 Ma after the onset of seafloor spreading, which would imply that rifting may cease at ~25 Ma (late Oligocene). Supported by the quantitative studies on the evolution and dynamics of the deepwater area of ZRMB, Dong et al. (2009) also demonstrated that rifting in the deepwater area of ZRMB postponed to 23 Ma. In this study, the subsidence rate after 33.9 Ma increased compared with the rate before (Fig. 4). This suggests that the rifting activity was still going on and the syn-rift stage was prolonged. According to Sun et al. (2009) and Franke (2013), the extension in the ZRMB initiated in the late Paleocene (around 59 Ma), with a climax during the late Eocene. Considering that the extension in the northern continental margin of the SCS migrated progressively from north to south (Cullen et al., 2010) and in light of the subsidence pattern (Fig. 4), we explain that the first rifting stage of the study area is during 49-33.9 Ma, initiated by the Zhuqiong Movement; the second rifting is during 33.9–23 Ma, triggered by the Nanhai Movement. The rifting division in this paper is in accordance with the result of Song et al. (2011).

5.2 *The Baiyun Movement*

Changes in subsidence rate of the study area can be related to the regional tectonic history of the ZRMB and episodes in the opening of the SCS. There is an important unconformity at ~23.8 Ma revealed by the ODP Site 1148, characterized by sharp changes in sediment geochemical parameters (Shao et al., 2004). This hiatus event was named Baiyun Movement by Pang et al. (2007). According to Pang et al. (2007), the Baiyun Movement was responsible for the rapid thermal subsidence that occurred at around 23.8 Ma in the Baiyun Sag and a change in the sedimentary environment from a continental shelf with neritic deposition to a continental slope with deepwater deposition since 23.8 Ma. The Baiyun Movement also marks an abrupt change of sediment provenance. Li et al. (2003) reported that sediment samples at ODP Site 1148 documented a rapid change in Nd isotopes and geochemistry at ca. 26–23 Ma, coinciding with a major discontinuity in the sedimentology and physical properties of the sediments. They compared the Nd isotopes of sediments from major rivers flowing into the South China Sea and suggested that pre-27 Ma sediments were dominantly derived from Indo China–Sunda Shelf and possibly northwestern Borneo, while post-23 Ma sediments were derived from South China. This change in provenance from southwest to north was interpreted to be related to a southward jump of spreading ridge in the South China Sea at ca. 25 Ma (Li et al., 2003).

Table 3. Calculated heat flow data (mW/m²) for all the wells used in this study

Well	49 Ma	38 Ma	33.9 Ma	23 Ma	19.1 Ma	16 Ma	10 Ma	5.3 Ma	0 Ma
a1	54.9	62.2	65.3	79.6	78.5	77.4	75.3	73.6	71.8
a2	54.9	65.3	69.8	87.8	85.8	84.0	80.7	78.3	75.8
a3	54.9	66.6	71.9	89.7	87.3	85.4	81.8	79.2	76.5
a4	54.9	63.6	67.4	88.9	86.9	85.1	81.7	79.1	76.5
a5	54.9	69.1	75.7	97.5	93.9	91.1	86.3	83.0	79.7
a6	54.9	62.9	66.4	92.3	89.9	87.8	83.9	81.1	78.2
a7	54.9	66.6	71.9	100.5	96.6	93.6	88.3	84.7	81.2
a8	54.9	65.5	70.2	101.0	97.1	94.1	88.7	85.0	81.5
a10	54.9	70.9	78.4	105.0	100.1	96.4	90.3	86.3	82.5
a11	54.9	68.0	74.0	100.7	96.7	93.6	88.2	84.6	81.1
a12	54.9	62.0	65.0	93.3	90.9	88.8	84.7	81.8	78.8
Average			70.5	94.2					78.5

This tectonic event can be recognized on the back-stripped tectonic subsidence curves in this study, characterized by a clear decrease in subsidence rate at 23.8 Ma (Fig. 4), which was previously noted by Clift and Lin (2001) as corresponding to the end of active extension in the ZRMB. The origin of the Baiyun Movement is not clear so far. It might be correlated to southward ridge jump in the South China Sea (Sun et al., 2008; Pang et al., 2009). Noted by Briais et al. (1993), the ridge jump occurred at the time of magnetic anomalies 6b–7, which are 25 Ma to 23 Ma according to the magnetic time scale of Cande and Kent (1995), and thus ended at the Baiyun Movement. However, the revised correlation of magnetic anomalies by Barckhausen and Roeser (2004) suggests the ridge jump at 25 Ma. The relation between the ridge jump and the Baiyun Movement has not yet been clarified and need more research.

6 Conclusions

In this study, a multi-stage finite stretching method has been used to unravel the tectono-thermal history of the Liwan Sag, which is important to understand the tectonic evolution as well as the hydrocarbon potential of this area. Our results suggest the following conclusions:

(1) The Liwan Sag has experienced a two-stage of rift and a subsequent post-rift stage since 49 Ma. The first rifting ranges from 49 Ma to 33.9 Ma, while the second rifting ranges from 33.9 Ma to 23 Ma. Since 23 Ma, the Liwan Sag has experienced a post-rift thermal subsidence stage.

(2) According to the above rifting and thermal subsidence stage, the Liwan Sag underwent a two-phase of heating and a subsequent persistent cooling until present. From 49 Ma to 33.9 Ma, the average basal heat flow increased from ~54.9 to ~70.5 mW/m^2; the second heating lasted from 33.9 Ma to 23 Ma, resulting in the average basal heat flow increasing from ~70.5 to ~94.2 mW/m^2. Finally, the Liwan Sag began to cooled down to its present thermal state since 23 Ma, with the current basal heat flow values ranging from ~71.8 to ~82.5 mW/m^2.

Acknowledgements

The authors are grateful to Chen Lin for the help on stretching factor and water depth estimation. We thank CNOOC for providing valuable basic data for this study.

References

Allen P A, Allen J R. 2005. Basin Analysis: Principles and Application. 2nd ed. Malden, MA: Blackwell Publishing, 560

Barckhausen U, Roeser H A. 2004. Seafloor spreading anomalies in the South China Sea revisited. In: Clift P, Kuhnt W, Wang P, et al., eds. Continent-ocean Interactions within East Asian Marginal Seas. Washington, DC: American Geophysical Union, 121–125

Bessis F. 1986. Some remarks on the study of subsidence of sedimentary basins Application to the Gulf of Lions margin (Western Mediterranean). Marine and Petroleum Geology, 3(1): 37–63

Briais A, Patriat P, Tapponnier P. 1993. Updated interpretation of magnetic anomalies and seafloor spreading stages in the South China Sea: implications for the Tertiary tectonics of Southeast Asia. Journal of Geophysical Research, 98(B4): 6299–6328

Cande S C, Kent D V. 1995. Revised calibration of the geomagnetic polarity timescale for the Late Cretaceous and Cenozoic. Journal of Geophysical Research, 10(B4): 6093–6095

Carminati E, Cavazza D, Scrocca D, et al. 2010. Thermal and tectonic evolution of the southern Alps (northern Italy) rifting: coupled organic matter maturity analysis and thermokinematic modeling. AAPG Bulletin, 94(3): 369–397

Chen Lin. 2014. Stretching factor estimation for the long-duration and multi-stage continental extensional tectonics: Application to the Baiyun Sag in the northern margin of the South China Sea. Tectonophysics, 611: 167–180

Chen Lin, Zhang Zhongjie, Song Haibin. 2013. Weak depth and along-strike variations in stretching from a multi-episodic finite stretching model: evidence for uniform pure-shear extension in the opening of the South China Sea. Journal of Asian Earth Sciences, 78: 358–370

Chen Sizhong, Pei Cunmin. 1993. Geology and geochemistry of source rocks of the eastern Pearl River mouth basin, South China Sea. Journal of Southeast Asian Earth Sciences, 8(1-4): 393–406

Clift P, Lin Jian. 2001. Preferential mantle lithospheric extension under the South China margin. Marine and Petroleum Geology, 18(8): 929–945

Cohen K M, Finney S, Gibbard P L. et al 2013. The ICS international chronostratigraphic chart. Episodes, 36(3): 199–204

Cramer B S, Toggweiler J R, Wright J D, et al. 2009. Ocean overturning since the Late Cretaceous: inferences from a new benthic foraminiferal isotope compilation. Paleoceanography, 24(4): PA4216

Cullen A, Reemst P, Henstra G, et al. 2010. Rifting of the South China Sea: new perspectives. Petroleum Geoscience, 16(3): 273–282

Dai Yiding, Pang Xiong. 1999. Petroleum geological characteristics of Zhu II Depression, Pearl River Mouth Basin. China Offshore Oil and Gas (Geology) (in Chinese), 13(3): 169–173

Ding Weiwei, Franke D, Li Jiabiao, et al. 2013. Seismic stratigraphy and tectonic structure from a composite multi-channel seismic profile across the entire Dangerous Grounds, South China Sea. Tectonophysics, 582: 162–176

Dong Dongdong, Zhang Gongcheng, Zhong Kai, et al. 2009. Tectonic evolution and dynamics of deepwater area of Pearl River mouth basin, Northern South China Sea. Journal of Earth Science, 20(1): 147–159

Falvey D A. 1974. The development of continental margins in plate tectonic theory. The APPEA Journal, 14(1): 95–106

Franke D. 2013. Rifting, lithosphere breakup and volcanism: comparison of magma-poor and volcanic rifted margins. Marine and Petroleum Geology, 43: 63–87

He Lijuan, Wang Kelin, Xiong Liangping, et al. 2001. Heat flow and thermal history of the South China Sea. Physics of the Earth and Planetary Interiors, 126(3-4): 211–220

He Lijuan, Xiong Liangping, Wang Jiyang. 2002. Heat flow and thermal modeling of the Yinggehai Basin, South China Sea. Tectonophysics, 351(3): 245–253

Hu Dengke, Zhou Di, Wu Xiangjie, et al. 2009. Crustal structure and extension from slope to deepsea basin in the northern South China Sea. Journal of Earth Science, 20(1): 27–37

Huang Chunju, Zhou Di, Sun Zhen, et al. 2005. Deep crustal structure of Baiyun Sag, northern South China Sea revealed from deep seismic reflection profile. Chinese Science Bulletin, 50(11): 1131–1138

Hudson S M, Hanson A D. 2010. Thermal maturation and hydrocarbon migration within La Popa Basin, northeastern Mexico, with implications for other salt structures. AAPG Bulletin, 94(3): 273–291

Jarvis G T, Mckenzie D P. 1980. Sedimentary basin formation with finite extension rates. Earth and Planetary Science Letters, 48(1): 42–52

Ji Mo, Zhang Gongcheng, Zhao Zhigang, et al. 2014. The tectonic evolution of Liwan sag in the deep-water area of the South China Sea and its oil geological significance. Geological Bulletin of China (in Chinese), 33(5): 723–732

Khain V E, Polyakova I D. 2004. Oil and gas potential of deep-and ultradeep-water zones of continental margins. Lithology and Mineral Resources, 39(6): 530–540

Kido Y, Suyehiro K, Kinoshita H. 2001. Rifting to spreading process along the northern continental margin of the South China Sea. Marine Geophysical Researches, 22(1): 1–15

Kominz M A, Browning J V, Miller K G, et al. 2008. Late Cretaceous to Miocene sea-level estimates from the New Jersey and Delaware coastal plain coreholes: an error analysis. Basin Research, 20(2): 211–226

Li Pinglu. 1993. Cenozoic tectonic movement in the Pearl River Mouth Basin. China Offshore Oil and Gas (Geology) (in Chinese), 7(6): 11–17

Li Xianhua, Wei Gangjian, Shao Lei, et al. 2003. Geochemical and Nd isotopic variations in sediments of the South China Sea: a response to Cenozoic tectonism in SE Asia. Earth and Planetary Science Letters, 211(3-4): 207–220

McKenzie D. 1978. Some remarks on the development of sedimentary basins. Earth and Planetary Science Letters, 40(1): 25–32

Miao Shunde, Zhang Gongcheng, Liang Jianshe, et al. 2013. Delta depositional system and source rock characteristics of Enping Formation, Liwan sag in ultra deep-water area of northern South China Sea. Acta Petrolei Sinica (in Chinese), 34(S2): 57–65

Miller K G, Mountain G S, Wright J D, et al. 2011. A 180-million-year record of sea level and ice volume variations from continental margin and deep-sea isotopic records. Oceanography, 24(2): 40–53

Nissen S S, Hayes D E, Buhl P, et al. 1995a. Deep penetration seismic soundings across the northern margin of the South China Sea. Journal of Geophysical Research, 100(B11): 22407–22433

Nissen S S, Hayes D E, Yao Bochu, et al. 1995b. Gravity, heat flow, and seismic constraints on the processes of crustal extension:

northern margin of the South China Sea. Journal of Geophysical Research, 100(B11): 22447–22483

Pang Xiong, Chen Changmin, Shao Lei, et al. 2007. Baiyun Movement, a great tectonic event on the Oligocene-Miocene boundary in the northern South China Sea and its implications. Geological Review (in Chinese), 53(2): 145–151

Pang Xiong, Chen Changmin, Zhu Ming, et al. 2009. Baiyun movement: a significant tectonic event on oligocene/miocene boundary in the Northern South China Sea and its regional implications. Journal of Earth Science, 20(1): 49–56

Peng Dajun, Pang Xiong, Chen Changmin, et al. 2005. From shallow-water shelf to deep-water slope-the study on deep-water fan systems in South China Sea. Acta Sedimentologica Sinica (in Chinese), 23(1): 1–11

Pettingill H S, Weimer P. 2002. Worlwide deepwater exploration and production: past, present, and future. The Leading Edge, 21(4): 371–376

Ru K, Pigott J D. 1986. Episodic rifting and subsidence in the South China Sea. AAPG Bulletin, 70(9): 1136–1155

Sclater J G, Christie P A F. 1980. Continental stretching: an explanation of the post-mid-Cretaceous subsidence of the central North Sea basin. Journal of Geophysical Research, 85(B7): 3711–3739

Shao Lei, Li Xianhua, Wang Pinxian, et al. 2004. Sedimentary record of the tectonic evolution of the South China Sea since the Oligocene: evidence from deep sea sediments of ODP Site 1148. Advances in Earth Science (in Chinese), 19(4): 539–544

Shi Xiaobin, Burov E, Leroy S, et al. 2005. Intrusion and its implication for subsidence: a case from the Baiyun Sag, on the northern margin of the South China Sea. Tectonophysics, 407(1-2): 117–134

Song Yang, Zhao Changyu, Zhang Gongcheng, et al. 2011. Research on tectono-thermal modeling for Qiongdongnan Basin and Pearl River Mouth Basin in the northern South China Sea. Chinese Journal of Geophysics (in Chinese), 54(12): 3057–3069

Steckler M S, Watts A B. 1978. Subsidence of the Atlantic-type continental margin off New York. Earth and Planetary Science Letters, 41(1): 1–13

Su Daquan, White N, McKenzie D A N. 1989. Extension and subsidence of the Pearl River Mouth Basin, northern South China Sea. Basin Research, 2(4): 205–222

Sun Zhen, Pang Xiong, Zhong Zhihong, et al. 2005. Dynamics of tertiary tectonic evolution of the Baiyun Sag in the Pearl River Mouth Basin. Earth Science Frontiers (in Chinese), 12(4): 489–498

Sun Zhen, Zhong Zhihong, Keep M, et al. 2009. 3D analogue modeling of the South China Sea: a discussion on breakup pattern. Journal of Asian Earth Sciences, 34(4): 544–556

Sun Zhen, Zhong Zhihong, Zhou Di, et al. 2008. Dynamics analysis of the Baiyun sag in the Pearl River mouth basin, North of the South China Sea. Acta Geologica Sinica, 82(1): 73–83

Tang Xiaoyin, Yang Shuchun, Hu Shengbiao. 2014. Thermal and maturation history of Jurassic source rocks in the Kuqa foreland depression of Tarim Basin, NW China. Journal of Asian Earth Sciences, 89: 1–9

Taylor B, Hayes D E. 1983. Origin and history of the South China sea basin. In: Proceedings of the 27th American Geophysical Union. Washington, DC: AGU

Wang Pinxian. 2012. Tracing the life history of a marginal sea-on "The South China Sea Deep" research program. Chinese Science Bulletin, 57(24): 3093–3114

Wang P, Prell W, Blum P, et al. 2000. Inital Reports, vol. 184. In: Proceedings of the Ocean Drilling Program. College Station, USA: ODP, Texas A&M

Wang Pinxian, Jian Zhimin, Zhao Quanhong, et al. 2003. Evolution of the South China Sea and monsoon history revealed in deep-sea records. Chinese Science Bulletin, 48(23): 2549–2561

Xie Hui, Zhou Di, Li Yuanping, et al. 2014. Cenozoic tectonic subsidence in deepwater sags in the Pearl River Mouth Basin, northern South China Sea. Tectonophysics, 615-616: 182–198

Xie Hui, Zhou Di, Pang Xiong, et al. 2013. Cenozoic sedimentary evolution of deepwater sags in the Pearl River Mouth Basin, northern South China Sea. Marine Geophysical Research, 34(3-4): 159–173

Xie Xinong, Müller R D, Li Sitian, et al. 2006. Origin of anomalous subsidence along the Northern South China Sea margin and its relationship to dynamic topography. Marine and Petroleum Geology, 23(7): 745–765

Yuan Yusong, Zhu Weilin, Mi Lijun, et al. 2009. "Uniform geothermal gradient" and heat flow in the Qiongdongnan and Pearl River Mouth Basins of the South China Sea. Marine and Petroleum Geology, 26(7): 1152–1162

Zhao Quanhong. 2005. Late Cainozoic ostracod faunas and paleoenvironmental changes at ODP Site 1148, South China Sea. Marine Micropaleontology, 54(1-2): 27–47

Zhou Di, Ru Ke, Chen Hanzong. 1995. Kinematics of Cenozoic extension on the South China Sea continental margin and its implications for the tectonic evolution of the region. Tectonophysics, 251(1-4): 161–177

Zhou Di, Sun Zhen, Liao Jie, et al. 2009. Filling history and post-breakup acceleration of sedimentation in Baiyun sag, deepwater northern South China Sea. Journal of Earth Sciences, 20(1): 160–171

Zhu Weilin, Li Mingbi, Wu Peikang. 1999. Petroleum systems of the Zhu III subbasin, Pearl River Mouth Basin, South China Sea. AAPG Bulletin, 83(6): 990–1003

Zhu Weilin, Zhong Kai, Li Youchuan, et al. 2012. Characteristics of hydrocarbon accumulation and exploration potential of the northern South China Sea deepwater basins. Chinese Science Bulletin, 57(24): 3121–3129